Computational Artifacts of the In-situ Electric Field in Anatomical Models Exposed to Low-Frequency Magnetic Field

Jose Gomez-Tames, Ilkka Laakso, *Member, IEEE*, Yuto Haba, Akimasa Hirata, *Fellow, IEEE*, Dragan Poljak, *Senior Member, IEEE*, and Kenichi Yamazaki, *Senior Member, IEEE*

Abstract— An *in-situ* (internal) electric field is used as a dosimetric quantity for human protection from low-frequency electromagnetic fields (lower than 5 MHz) under international safety standard/guidelines. The IEEE standard uses a homogenous elliptical cross section to derive external field strength corresponding to an *in-situ* field strength, while the International Committee on Non-Ionizing Radiation Protection (ICNIRP) guidelines use anatomical models to relate them. In the latter, "the 99th percentile value of the *in-situ* electric field averaged over the cube of its side length of 2 mm" is used to represent the maximum in-situ electric field. This metric was introduced to suppress computational artifacts that are inherent when using voxelized anatomical models, in which curved boundaries are discretized with a stair-casing approximation. To suppress the error, a few schemes have been proposed for treating the computational artifacts. In this study, the various schemes to suppress the artifacts are reviewed. Subsequently, a post-processing method for determining the appropriate maximum *in-situ* field strength is proposed. The performance of the proposed scheme is first verified by comparison with an analytical solution in a multi-layered sphere. The method is then applied for different exposure scenarios in anatomically realistic human models where the volume under computation is also considered.

Index Terms— dosimetry, biological effects of electromagnetic field, standardization, blood flow measurement, simulation

I. INTRODUCTION

THERE have been concerns about adverse health effects caused by human exposure to electromagnetic fields.

Under international standards/guidelines [1], [2], the internal (*in-situ*) electric field is used as a dosimetric quantity for human protection against fields at frequencies lower than 5 MHz [1] or 10 MHz [2].

In the IEEE standard [1], the allowable external field strength (maximum permissible exposure/exposure reference level) is determined using a homogeneous ellipsoid to relate to the allowable internal (or *in-situ*) electric field strength (dosimetric reference level [3]). In the guidelines of the International Commission on Non-Ionizing Radiation Protection (ICNIRP), the relation between the *in-situ* and external field strengths are determined by referring to published data of calculations that utilized voxelized anatomical human models [4]–[6]. One of the disadvantages of using voxelized anatomical human models is that computed *in-situ* fields, especially around the model surface, suffer from computational artifacts. The 99th percentile value of the field strength is considered to remove computational artifact. In addition, the field strength averaged over a cube of 2 mm should be considered for the same purpose. The ICNIRP guidelines [2] say '*For a specific tissue, the 99th percentile value of the electric field is the relevant value to be compared with the basic restriction. As a practical compromise, satisfying requirements for a sound biological basis and computational constraints, ICNIRP recommends determining the induced electric field as a vector average of the electric field in a small contiguous tissue volume of 2×2×2 mm³.*' A reduction factor of three regarding the computational uncertainty is then considered.

Under these circumstances, the suppression of numerical artifacts and the reduction factor are listed in the research agenda of the IEEE International Committee on Electromagnetic Safety (ICES) [7]. A working group on 'numerical artifacts' has been established in IEEE ICES to clarify certain aspects. This working group has two missions: (i) to compute induced electric fields in conformal and voxel models and (ii) to suppress the computational error in the voxel model. In this study, our discussion focuses on the latter aspect.

The computational artifacts in the anatomical model for uniform exposure is less than 10% when considering the 99th percentile value [8]. The 99th percentile value was proposed in [9] and then applied in [10]. The value of the 99th percentile should be noteworthy, in that it can provide an approximation of the *in-situ* field strength for uniform exposure. The application of the 99th percentile for non-uniform exposure is worth discussing for defining the limitations [11], as well as appropriate compliance of product safety [12] because, in some domestic/regional regulations, the descriptions in the international standard/guidelines are directly adopted.

Until now, there have been a few methods to suppress the computational artifacts in the voxelized human model. In [13], an algorithm for smoothing tissue conductivity in anatomical models is proposed considering the error in developing a voxel human model (tissue boundary classification). The algorithm works well for both uniform and non-uniform exposures. One of the drawbacks is that it is not applicable for the results obtained by commercial software. In [14], the 99.9[th] percentile value is used for localized exposure. This was also used in some dosimetric studies (e.g., [15]). The 99.9[th] percentile is rather arbitrary, although it is more appropriate than the 99th percentile, at least for a non-uniform exposure. Further discussion is needed for systematic evaluation.

Another issue related to the ICNIRP guidelines is that the field strength averaged over $2\times2\times2$ mm^3 cube is discussed using finer voxel resolutions. For a homogeneous sphere, the field strength of a 2-mm cube is stable at model resolutions finer than 2 mm [16]; no discussion has been given regarding inhomogeneous and realistic models.

In this study, we have made a comparison of previous pre- and post-processing schemes (smoothing, 99.9[th] percentile, 99th percentile, and $2\times2\times2$ mm^3) for the results in multi-layer spheres and anatomical models. Also, a new post-processing method, that is applicable to the results obtained by any commercial software, is proposed and compared with previous schemes. As a non-uniform field source, a magnetic dipole and loop current are considered.

II. Models and Methods

A. Human Models and Exposure Scenarios

To evaluate the scheme for suppressing the numerical artifact, a multi-layer sphere exposed to a quasi-static magnetic field of an infinitesimally short magnetic dipole is considered. The magnetic dipole is located 60 or 200 mm away from the sphere (see Fig. 1). The analytical solution for this kind of geometry can be obtained from the Maxwell equations using the Mie solution. The multilayered sphere consists of 9 layers: skin (80 mm of radius and 2.0×10^{-4} S/m of conductivity), fat (76 mm, 0.043 S/m), muscle (74 mm, 0.34 S/m), skull (72 mm, 0.02 S/m), muscle (68 mm), cerebrospinal fluid (66 mm, 2.0 S/m), brain (64 mm, 0.11 S/m), cerebrospinal fluid (42 mm), and brain (38 mm)   [13]. The sphere was discretized with resolutions of 0.5, 1.0, or 2.0 mm.

As anatomical models, TARO (Japanese adult male model) [17], and Duke (European adult male model) from the Virtual Family [18] are used. Considering the magnetic field exposure from an electric shaver, a one-loop coil is located 30 mm from the chin. The current flowing through the coil is 1 A.

B. Scalar-potential finite-difference equation

A poorly conducting object, such as the human body, is exposed to an external low-frequency magnetic field. For frequencies lower than the MHz range, the induced current can be assumed not to perturb the external magnetic field. The electric scalar potential can be solved [19], [20] using the scalar-potential equation:
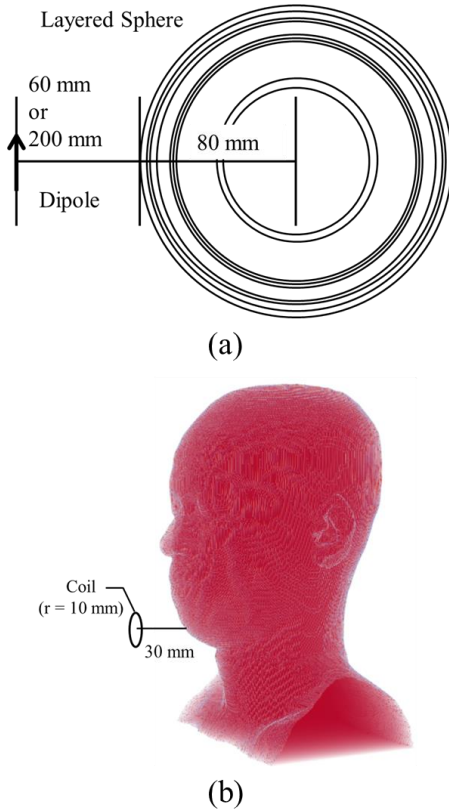

Fig.1. (a) Multi-layer sphere exposed to a magnetic dipole and (b) anatomical head model exposed to a loop current.

$$\nabla \cdot \sigma\nabla\varphi = -\nabla\sigma\frac{d}{dt}A_0. \qquad (1)$$

The vector potential, A_0, can be calculated using the Biot–Savart law, or by selecting a suitable value for A_0 when the incident magnetic flux density, B_0, is simple.

C. Finite-Element Method

Equation (1) is solved numerically using the finite-element method (FEM) with trilinear node-based basis functions in cubical elements. The matrix equation is solved iteratively by the successive over-relaxation (SOR) iteration. Compared to the SPFD method [21], the finite-element formulation used in this study requires more operations (21 non-zeros on each row of the system matrix compared to 7 in the SPFD method), but the SOR iteration converges slightly faster. The numerical accuracy (verified using the layered sphere of Fig. 1a) and memory requirements of the two methods are similar.

III. Pre- or Post-processing Methods of computed *in-situ* electric field

A. Proposal of the Post-Processing Method

As mentioned above, the voxel maximum of an *in-situ* electric field is affected by the stair-casing error, especially at the tissue boundary with a high conductivity contrast. It is

essential to know how to define this computational artifact systematically (outliers).

In this study, the outliers are found and post-processed using a polynomial approximation. First, we define the voxel *in-situ* electric field E_n, as the *n*-th element of the list of the electric field values sorted in the ascending order (Fig. 2). The gradient Δ is computed for each E_n by the following equation:

$$\Delta_n = \frac{E_{n+1} - E_n}{(E_n + E_{n+1})/2}, \qquad (2)$$

The first significantly different value of the gradient is defined as the detection point of the outlier (Fig. 2). To find it, the frequency distribution of the gradient is investigated in an outlier detection method with quartiles (Fig. 3). The reason for using the quartile method is that it is a stable static, which is less sensitive to outliers. Specifically, it is required just to have a single peak and fair symmetry in the distribution (even in normal or logarithm scales) to apply the interquartile approach
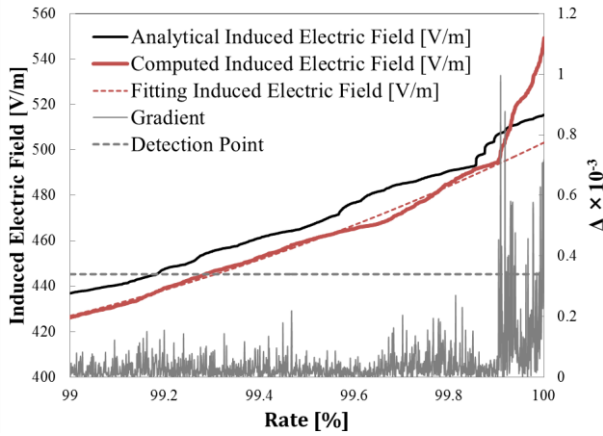

Fig.2. Computed results of induced field strength and gradient for voxels whose field strength has the 1% highest value in the multi-layer sphere. For comparison, analytical results and estimated value are also presented. The computed and analytical electric fields are sorted in ascending order from the 99 to 100% percentiles.
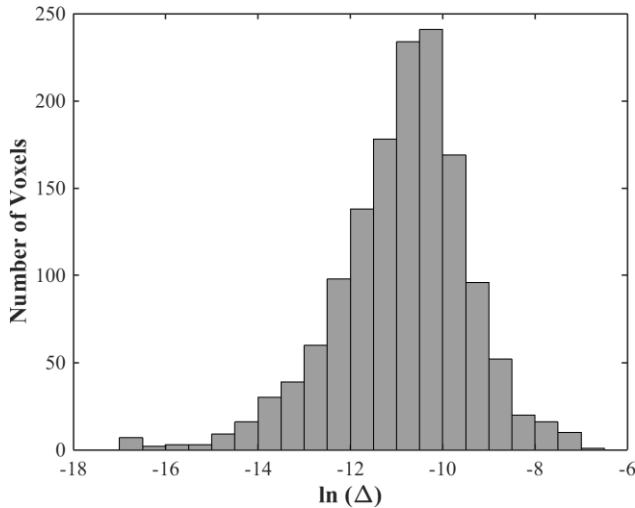

Fig.3. Frequency distribution ln (Δ) in the skin and fat of the layered sphere according to eq. (2). In this case, the detection point (3σ) of the outlier is $e^{-8} = 0.34 \times 10^{-3}$.

considered here. The outlier in the dosimetric studies can be assumed to be less than 1%, as shown in ICNIRP [2], and thus the *in-situ* electric field values for only the highest 1% (99 to 100 %) are processed statistically.

Here we discuss the procedure for finding the outlier based on [22]. The detection point of the outlier considered in this study is triple the standard deviation (3σ) or 99.73%. Also, it can be obtained by calculating:

$$\text{Detection Point} = \mu + 2.44 \times IQR \qquad (3)$$

where μ is the mean and IQR is the interquartile range of the frequency distribution in Fig. 3. Note that 3σ is equal to $2.44 \times IQR$.

The first point of the gradient exceeding the detection point is set as the outlier detection percentile, as shown in Fig. 2. The voxels, sorted in ascending order, whose electric fields are larger than the threshold, are substituted by the value estimated in terms of the second polynomial approximation. Note that the approximation was derived from the field strength from the 99th percentile value to the first point where the gradient exceeds the threshold for the first time.

B. Pre-processing Method

Large contrasts in tissue conductivity between neighboring voxels have been suggested as the main reason for the staircase approximation error [4], [9], [23]. The pre-processing algorithm for reducing the staircase approximation error consists of simply making the conductivity smoother to reduce contrast, thus making the problem easier to solve numerically [13]. The newly smoothed conductivity, σ_{smooth}, in each voxel is a linear average of the original conductivity, σ_{old}, over a spherical volume

$$\sigma_{\text{smooth}}(i_0, j_0, k_0) = \frac{1}{N} \sum_{i,j,k \in S_n} \sigma_{\text{old}}(i, j, k), \qquad (4)$$

where S_n is a voxelized sphere centered at the voxel (i_0, j_0, k_0), consisting of a total of N voxels, with a radius (the 'smoothing radius') of n voxels. Based on the findings of the previous study [13], we chose $n=3$ in this study which is optimal to reduce the artifacts. If a large n is chosen, some drawbacks of the smoothing method may become significant: i) a small conductivity is assigned to air voxels near the body and ii) loss of anatomical details.

C. Electric Field Averaged over a $2 \times 2 \times 2$ mm³ Cube

The ICNIRP guidelines [2] require us to take a vector average of the electric field over $2 \times 2 \times 2$ mm³ cubes. In this study, three resolutions of the cube, i.e., 0.5, 1, and 2 mm, were considered. For the voxel resolution of 2 mm, the ICNIRP-averaged electric field in each voxel is the same as the electric field value at the center point of the voxel. For the resolution of 0.5 and 1 mm, the induced electric field is averaged over 8 and 64 voxels, respectively. For the analytical solutions in section III.*A*, the ICNIRP average of the analytical electric field was approximated as the pointwise electric field value at the center of each voxel.

IV. RESULTS AND DISCUSSION

A. Application of Proposed Method to the Multi-layer Sphere Exposure from Magnetic Dipole.

Figure 2 shows computed results for the *in-situ* field strength in the multi-layer sphere. From this figure, it can be seen that the computed *in-situ* field is smaller than that of the analytical solution for the 99.9th percentile or lower. The computed electric field higher than the 99.9th percentile exceeds the rapidly analytical solution. The gradient is larger than the threshold value around this percentile. The *in-situ* electric field higher than that percentile is considered to be the outlier by the definition in the Sec. III. A.

Fig. 3 shows the frequency distribution of the gradient of the electric field *in-situ* in the multi-layer sphere with a resolution of 2 mm. The frequency of the voxel *in-situ* electric field sorted in the ascending order (in the range from 99 to 100%) has a distribution with a single peak and fair symmetry in the logarithmic scale, which is used to determine the detection point value [22]. From the second polynomial approximation for the *in-situ* electric fields from 99% to the detection point (99.87% in this case), the *in-situ* electric field at points higher than the percentile can be extrapolated (see also Fig. 2). Figure 4 shows the electric field distribution on the surface of the multi-layer sphere obtained by the proposed algorithm as well as the analytical and computed results. As shown in Fig. 4, the induced electric field obtained by the proposed method is in good agreement with the analytical solution.
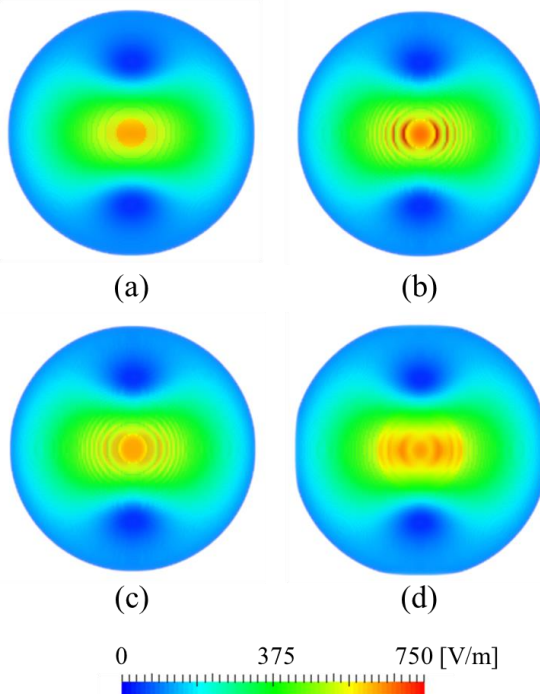

Fig.4. Electric field on the surface of the multi-layer sphere for non-uniform exposure; (a) analytical, (b) computed, (c) proposed post-processing, and (d) pre-processing smoothing methods.

B. Pre- and Post-Processing Methods Performance in Multi-layer Sphere Model

To confirm the effectiveness of our proposal, Table 1 lists the estimated percentage error of the *in-situ* electric field for different methods during non-uniform exposure. In the proposed method, the detection point was also presented. From this table, it can be seen that the computed maximum *in-situ* electric fields are up to 64% larger than those of the analytical values. This tendency becomes obvious for the computation with fine resolution models in Table 1. This is because the singularity becomes significant for finer resolutions as pointed out in [9].

As mentioned above, the ICNIRP guidelines recommend *"determining the induced electric field as a vector average of the electric field in a small contiguous tissue volume of 2×2×2 mm3."* However, this volume-averaged value provides some suppression of singular values when compared to the original resolution; for a resolution of 0.5 mm, the difference between the computed and analytical maximum field strength is suppressed by 8−15 points. This result is different from the findings in [16] that state that an induced field strength is stable for resolutions lower than 2 mm, in which a homogeneous sphere was used (unlike the multi-layered sphere in this study).

From Table 1, the values obtained by the proposed and 99.9th methods, as well as the smoothing method are in better agreement with the analytical value than with the volume average value by the 2×2×2 mm3 or 99th percentile. The difference between the analytical solution and computed results with a smoothing algorithm was lower than the others in most cases. This is because the tissue boundary with a high conductivity contrast is avoided as discussed in [13]. The maximum difference between the analytical and proposed algorithm at a distance of 60 mm appeared in the grey matter where the boundary with the CSF existed. In general, the error was higher in grey matter and cortical bone than other tissues and lower in muscle and cerebrospinal fluid. Additionally, the proposed and 99.9th percentile methods had better performance than smoothing with a finer resolution if the smoothing radius is not adjusted.

The maximum *in-situ* electric field estimated by the proposed method is larger than that of the 99.9th percentile. This is because the detection percentile for the outlier is larger than the 99.9 percentile in most cases. Specifically, the percentile of outlier detection was variable from 99.86 to 99.99%. The border percentiles of the outliers are comparable to each other at a distance of 60 mm (average value is 99.948% for the resolution of 0.5 mm while 99.952% at 2 mm). Conversely, the border percentile gradually increased at a distance of 200 mm: 99.920% at 0.5 mm and 99.968% at 2 mm. In general, the proposed method presents a smaller error than the 99.9th percentile using a high-resolution model and short distance of non-uniform exposure. In contrast, the 99th percentile method unperformed for short distance exposure.

C. Pre- and Post-Processing Methods Computed in Limited Volume

Including   model   regions   in   the   computation   of percentile-based methods that are far from the exposure site

Table 1. Error between analytical and computed electric field strength in non-uniform exposure. Proposed algorithm, 99.9th percentile, and 99th percentile are applied for computed *in-situ* electric field. In addition, the smoothing algorithm is applied as a pre-processing. Also shown is the field strength averaged over $2\times2\times2$ m^3 cube: Model resolution of 0.5 mm for the model-source distance of (a) 60 mm and (b) 200 mm, model resolution of 1 mm for the model-source distance of (c) 60 mm and (d) 200 mm, model resolution of 2 mm for the model-source distance of (e) 60 mm and (f) 200 mm.

| Tissue	Singular point [%]	Proposed [%]	99.9% ile [%]	99.0% ile [%]	Smoothing [%]	$2\times2\times2$ mm^3 cube [%]	Maximum [%]
(a) 0.5 mm, 60 mm							
Skin and Fat	99.956	-3.9	-6.4	-21.4	7.3	19.4	29.2
Muscle	99.962	-1.5	-3.6	-17.2	1.5	5.3	15.3
Cortical Bone	99.940	4.4	2.1	-19.2	7.1	33.1	46.1
Cancellous Bone	99.964	-3.9	-6.0	-18.1	1.5	3.7	14.1
CerebroSpinal Fluid	99.927	-1.4	-3.1	-19.3	5.0	18.6	26.6
Grey Matter	99.939	-4.7	-7.7	-28.7	11.2	47.3	55.5
(b) 0.5 mm, 200 mm							
Skin and Fat	99.913	4.9	3.7	-7.6	8.9	12.7	30.3
Muscle	99.920	5.7	4.8	-5.9	2.8	11.4	16.2
Cortical Bone	99.954	22.3	18.1	-4.0	7.1	30.4	45.7
Cancellous Bone	99.922	-0.2	-0.9	-7.5	2.8	4.3	15.0
CerebroSpinal Fluid	99.922	6.1	4.7	-7.6	6.0	12.8	27.3
Grey Matter	99.889	-0.6	0.9	-13.3	12.0	41.0	54.8
(c) 1 mm, 60 mm							
Skin and Fat	99.970	0.5	-3.1	-20.9	2.9	15.2	24.5
Muscle	99.909	-2.4	-4.1	-17.3	0.8	2.4	6.6
Cortical Bone	99.973	14.7	9.8	-14.6	1.1	32.3	44.3
Cancellous Bone	99.971	-2.8	-5.1	-17.6	1.4	3.8	10.4
CerebroSpinal Fluid	99.924	1.8	0.5	-19.4	2.8	16.8	22.4
Grey Matter	99.944	1.9	-1.5	-27.4	5.0	36.4	60.9
(d) 1 mm, 200 mm							
Skin and Fat	99.967	14.1	10.1	-6.7	6.5	14.9	27.2
Muscle	99.959	9.2	5.9	-6.1	1.2	8.2	13.9
Cortical Bone	99.885	26.8	25.6	1.2	1.0	33.3	44.4
Cancellous Bone	99.945	3.5	1.9	-7.3	3.6	6.1	12.1
CerebroSpinal Fluid	99.953	14.1	10.0	-7.9	2.8	15.6	23.4
Grey Matter	99.941	15.0	11.6	-12.2	6.5	47.3	59.5
(e) 2 mm, 60 mm							
Skin and Fat	99.865	0.3	1.1	-20.1	0.6	19.6	27.9
Muscle	99.983	-8.1	-9.8	-19.2	0.3	-11.6	-3.5
Cortical Bone	99.939	10.6	8.0	-10.4	-0.7	23.3	28.6
Cancellous Bone	99.983	-3.8	-7.0	-16.6	0.9	-0.6	6.2
CerebroSpinal Fluid	99.970	-6.6	-7.7	-20.8	0.3	-8.9	-2.3
Grey Matter	99.969	17.7	10.0	-25.0	1.3	44.1	55.2
(f) 2 mm, 200 mm							
Skin and Fat	99.971	21.5	17.8	-2.7	1.5	16.2	34.6
Muscle	99.983	-0.8	-2.5	-10.1	1.0	-12.2	1.4
Cortical Bone	99.939	31.5	28.1	7.1	1.2	23.5	43.5
Cancellous Bone	99.990	3.3	2.1	-5.8	3.1	-8.6	5.4
CerebroSpinal Fluid	99.970	2.4	-0.5	-10.1	2.6	-6.7	4.8
Grey Matter	99.953	30.6	23.1	-9.6	3.9	49.6	64.2
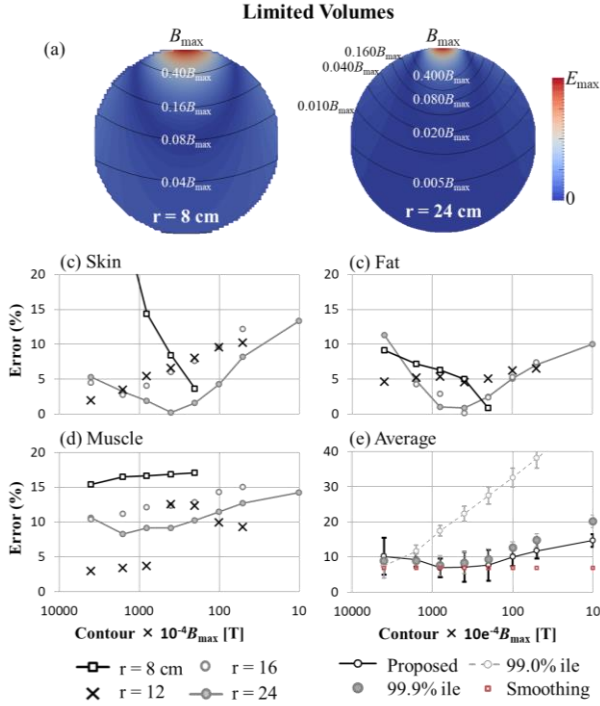
Fig.5. Effect of model size and limited volume on the methods' performance during non-uniform exposure. a) Limited volumes enclosed by contours in the spherical model of 2 mm of resolution. b-d) Error between the analytical solution and numerical computation of the electric field by the proposed method. e) Average error of pre- and post-processing methods.

Fig.6. Limited volume and performance of pre- and post-processing methods applied to TARO model during non-uniform exposure.

may reduce the performance of the methods. The reason for this is that more voxels would be removed during the post-processing computation with a possible overestimation of the actual number of artifacts. To evaluate this issue, the results obtained using different methods were compared with the analytical solution on various tissues of the multi-layer spherical model with maximum radii of 8, 12, 16, and 24 cm. The source was a magnetic dipole located 60 mm from the model.

As shown in Figs. 5b to 5d, the error increases with the volume. The error can be minimized to less than 15% by limiting the volume with contours where the magnetic field is a fraction of its maximum strength inside the model (B_{max}) (see Fig. 5a) by using a contour between $0.01B_{max}$ and $0.1B_{max}$. Additionally, the average performance between the smooth, proposed and 99.9th methods are comparable in Fig. 5e. In the same figure, an error lower than 10% can be attained by limited volumes between $0.01B_{max}$ and $0.1B_{max}$. Unlike the proposed method and the 99.9th percentile approach, the 99th approach was significantly sensitive to both the volume and the total number of voxels in the model.

The benefit of using the limited volume approach is more significant in larger models, such as the full human body. For instance, the error in a sphere of radius $r = 24$ cm is reduced by at least 15, 11, and 8 points for skin, fat, and muscle,
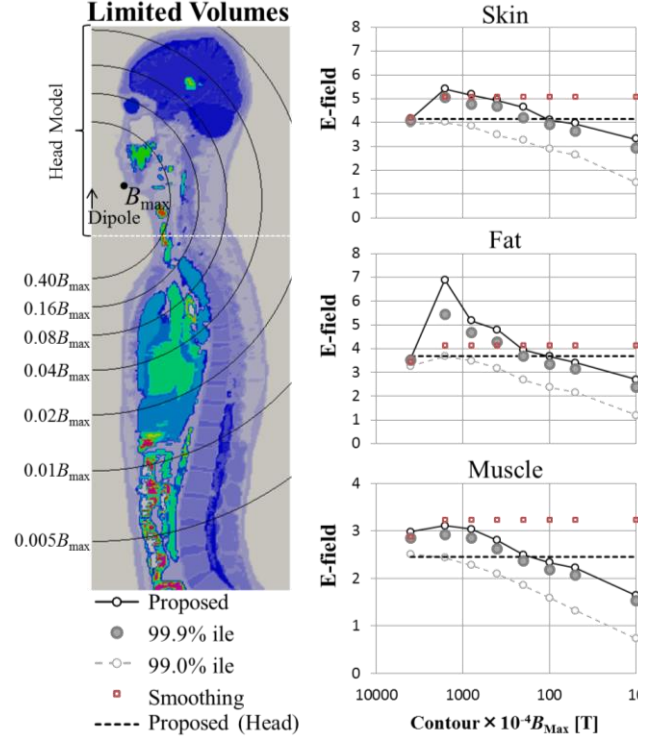
respectively. This is achieved by applying any contour between $0.01B_{max}$ and $0.1B_{max}$. For the sphere representing the head model ($r = 8$ cm, section IV.B), the minimum error is achieved using the contour $0.02B_{max}$ that is within the proposed range and corresponds to the full volume.

D. Application of Algorithms to Realistic Human Models

Table 2 shows the estimated maximum value of the *in-situ* electric field from non-uniform exposure using the proposed, smoothing and 99.9th percentile methods as well as the 99th percentile value. Note that the frequency distribution of Δ is similar to Fig. 3 in TARO with a resolution of 2 mm. The frequency distribution roughly followed the logarithmic normal distribution, and thus proposal is applicable.

As seen in Table 2, the 99.9th percentile and smoothing algorithm provided the lowest and highest values between all methods, respectively, in all the cases. However, it is impossible to conclude which methods provided best estimates because no analytical solution exists. Instead, the point to be stressed here is that the computational uncertainty between the maximum computed field strength and those obtained by proper pre- or post-processed methods would be much smaller than a factor of three in full body, which is given in the ICNIRP guidelines [2]. This difference is larger than that observed in the sphere or the limited volume approach for the anatomical model (factor 1 to 1.5). This is because of the complicated anatomy as well as morphology in the human, which is also attributable to being discretized by finite voxels.

Table 2. Computed electric field strength by the pre- and post-processing methods in human model: (a) TARO and (b) Duke.

Tissue	Singular point [%]	Proposed [V/m]	99.9% ile [V/m]	99.0% ile [V/m]	Smoothing [V/m]	Maximum [V/m]
(a)						
Skin	99.969	6.34	5.55	2.81	9.69	10.53
Muscle	99.948	3.33	3.10	1.49	6.37	6.46
Fat	99.960	5.19	4.58	2.29	7.96	11.26
Cortical Bone	99.964	4.68	4.15	2.28	5.78	7.36
Cancellous Bone	99.991	3.78	3.29	1.45	5.47	6.43
(b)						
Skin	99.975	6.73	5.91	2.52	7.23	13.65
Muscle	99.977	3.21	2.68	0.93	3.47	8.39
Fat	99.983	5.06	4.34	1.69	6.10	11.62
Cortical Bone	99.959	5.71	5.27	3.12	6.36	11.82
Cancellous Bone	99.990	4.55	3.97	2.30	5.20	7.44

Table 3. Performance of the pre- and post-processing methods applied to TARO model during uniform exposure.

Tissue	Singular point [%]	Proposed [V/m]	99.9% ile [V/m]	99.0% ile [V/m]	Smoothing [V/m]	Maximum [V/m]
Skin	99.993	4.88	3.76	0.80	4.67	8.45
Muscle	99.923	0.57	0.56	0.44	0.97	1.58
Fat	99.950	1.33	1.24	0.83	1.82	3.61
Cortical Bone	99.966	1.71	1.58	1.06	1.52	3.38
Cancellous Bone	99.976	1.10	1.01	0.71	1.32	1.78

Also, the smaller uncertainty of the calculation of the *in-situ* electric field between methods (proposed, 99.9th, and smoothing), the more confidence we can have in the results. When comparing the results between TARO and Duke, the former has a variation of 16−35% while the latter has a variation between 9−17%. So, the inter-individual variability of the *in-situ* electric field may also be large between models. In addition, the variation can be reduced to less than 15% if the limited volume is used between $0.02B_{max}$ and $0.1B_{max}$, as shown in Fig. 6. If the selected volume is the head, the variation is also 15%. Note that the limited volume range ($0.02B_{max}$ and $0.1B_{max}$) is in agreement with the range presented in section IV.*C* for the spherical model.

In the case of the uniform-field exposure in Table 3, the proposed algorithm was applicable to obtain the singular point for each tissue in realistic human models. The maximum electric field strength obtained by the proposed method is comparable to the smoothing and is larger than 99.9th and 99th percentiles. The 99th percentile can be taken as a conservative value in the sphere for a uniform-field exposure [9].

V. SUMMARY

In this study, pre- and post-processing methods for removing numerical artifacts in the dosimetry of human exposure to low-frequency magnetic field have been discussed. This numerical artifact is inherent when using voxel models. To resolve this issue, using conformal model would be essential but at the same time more demanding. This is crucial when considering non-uniform, whole-body exposure with high-resolutions [24], [25].

First, the analytical solution of a multi-layered sphere is compared with five schemes for removing computational artifacts in this study. The proposed method, pre-processing smoothing, and 99.9th percentile had comparable performances. The proposed method has been particularly good at short distances of non-uniform exposure and optimal for models with fine resolutions (0.5 mm). In contrast, the 99th percentile approximation unperformed with short distance exposure. Additionally, averaging over a $2\times2\times2$ mm³ volume was not the best for inhomogeneous models, with up to 20% error.

Second, the performance of the methods can be improved by considering different volumes inside the model during non-uniform exposure. It was found that volumes limited by contours, where the magnetic field is between 2% and 10% of its maximum strength, can reduce the error by one order of magnitude in the proposed and 99.9th percentile methods.

Third, the selection of the most accurate method is not possible for realistic models because no analytical solutions exist. However, the computational uncertainty in the computed field strength with proper pre- or post-processing is smaller than a factor of three, which can be reduced to 1.5 or smaller if the limited volume method is used (factors in accordance with ICNIRP guidelines [2]) in non-uniform exposure. Furthermore, the variability between the pre- and post-processing methods is 35% for a full body, and suppressed to be less than 15% for the limited volume approach using the same contour range obtained in the spherical study. The effect of voxel resolution on the calculation of in-situ field for realistic models can be addressed in future work to investigate if the computation uncertainty is reduced between proposed method, 99th and smoothing, in particular at shorter model-source distance and finer voxel resolution for non-uniform exposure, as derived from the results using spherical model

Finally, in order to maximize the reduction of the computational error in the voxel models, a revision of the $2\times2\times2$ mm³ metric should be considered while the proposed and 99.9th methods and the limited volume approach can be adopted for their better performance in model resolution and exposure distances in the non-homogenous model and non-uniform exposure.

ACKNOWLEDGMENT

REFERENCES

[1] IEEE International Committee on Electromagnetic Safety on Non-Ionizing Radiation., Institute of Electrical and Electronics Engineers., and IEEE-SA Standards Board., *IEEE standard for safety levels with respect to human exposure to electromagnetic fields, 0-3kHz*. Institute of Electrical and Electonics Engineers, 2002.

[2] ICNIRP, "Guidelines for limiting exposure to time-varying electric, magnetic, and electromagnetic fields (up to 300 GHz). International Commission on Non-Ionizing Radiation Protection.," *Health Phys.*, vol. 74, no. 4, pp. 494–522, Apr. 1998.

[3] IEEE International Committee on Electromagnetic Safety. Technical Committee 95., Institute of Electrical and Electronics Engineers., and IEEE-SA Standards Board., *IEEE standard for military workplaces--force health protection regarding personnel exposure to electric, magnetic, and electromagnetic fields, 0 Hz to 300 GHz.* .

[4] P. Dimbylow, "Development of the female voxel phantom, NAOMI, and its application to calculations of induced current densities and electric fields from applied low frequency magnetic and electric fields," *Phys. Med. Biol.*, vol. 50, no. 6, pp. 1047–1070, Mar. 2005.

[5] P. Dimbylow, "Development of pregnant female, hybrid voxel-mathematical models and their application to the dosimetry of applied magnetic and electric fields at 50 Hz," *Phys. Med. Biol.*, vol. 51, no. 10, pp. 2383–2394, May 2006.

[6] Z. Xiong, S. Feng, R. Kautz, S. Chandra, N. Altunyurt, and J. Chen, "Multi-GPU Accelerated Admittance Method for High-Resolution Human Exposure Evaluation," *IEEE Trans. Biomed. Eng.*, vol. 62, no. 12, pp. 2920–2930, Dec. 2015.

[7] J. P. Reilly and A. Hirata, "Low-frequency electrical dosimetry: research agenda of the IEEE International Committee on Electromagnetic Safety," *Phys. Med. Biol.*, vol. 61, no. 12, pp. R138–R149, Jun. 2016.

[8] A. Hirata, K. Yamazaki, S. Hamada, Y. Kamimura, H. Tarao, K. Wake, Y. Suzuki, N. Hayashi, and O. Fujiwara, "Intercomparison of induced fields in Japanese male model for ELF magnetic field exposures: effect of different computational methods and codes," *Radiat. Prot. Dosimetry*, vol. 138, no. 3, pp. 237–244, Mar. 2010.

[9] T. Dawson, M. Potter, and M. Stuchly, "Evaluation of modeling accuracy of power frequency field interactions with the human body," *Appl. Comput. Electromagn. Soc. J.*, vol. 16, pp. 162–172, 2001.

[10] A. Hirata, K. Caputa, T. W. Dawson, and M. A. Stuchly, "Dosimetry in models of child and adult for low-frequency electric field," *IEEE Trans. Biomed. Eng.*, vol. 48, no. 9, pp. 1007–1012, 2001.

[11] V. De Santis, X. L. Chen, and International Commission on Non-Ionizing Radiation Protection, "On the issues related to compliance assessment of ICNIRP 2010 basic restrictions," *J. Radiol. Prot.*, vol. 34, no. 2, pp. N31–N39, Jun. 2014.

[12] Y. Diao, K. H. Chan, S. W. Leung, W. Sun, and Y. M. Siu, "Prediction of magnetic field emissions by current source reconstruction using radial basis function network," *Electron. Lett.*, vol. 51, no. 16, pp. 1243–1245, Aug. 2015.

[13] I. Laakso and A. Hirata, "Reducing the staircasing error in computational dosimetry of low-frequency electromagnetic fields," *Phys. Med. Biol.*, vol. 57, no. 4, pp. N25–N34, Feb. 2012.

[14] B. Kos, B. Valič, D. Miklavčič, T. Kotnik, and P. Gajšek, "Pre- and post-natal exposure of children to EMF generated by domestic induction cookers," *Phys. Med. Biol.*, vol. 56, no. 19, pp. 6149–6160, Oct. 2011.

[15] I. Laakso and A. Hirata, "Evaluation of the induced electric field and compliance procedure for a wireless power transfer system in an electrical vehicle," *Phys. Med. Biol.*, vol. 58, no. 21, pp. 7583–7593, Nov. 2013.

[16] X.-L. Chen, S. Benkler, N. Chavannes, V. De Santis, J. Bakker, G. van Rhoon, J. Mosig, and N. Kuster, "Analysis of human brain exposure to low-frequency magnetic fields: A numerical assessment of spatially averaged electric fields and exposure limits," *Bioelectromagnetics*, vol. 34, no. 5, pp. 375–384, Jul. 2013.

[17] T. Nagaoka, S. Watanabe, K. Sakurai, E. Kunieda, S. Watanabe, M. Taki, and Y. Yamanaka, "Development of realistic high-resolution whole-body voxel models of Japanese adult males and females of average height and weight, and application of models to radio-frequency electromagnetic-field dosimetry.," *Phys. Med. Biol.*, vol. 49, no. 1, pp. 1–15, Jan. 2004.

[18] A. Christ, W. Kainz, and E. Hahn, "The Virtual Family—development of surface-based anatomical models of two adults and two children for dosimetric simulations," *Phys. Med. Biol.*, vol. 55, no. 2, 2010.

[19] T. Dawson and M. Stuchly, "Analytic validation of a three-dimensional scalar-potential finite-difference code for low-frequency magnetic induction," *Appl. Comput. Electromagn. Soc. J.*, vol. 11, pp. 72–81, 1996.

[20] T. W. Dawson and M. A. Stuchly, "High-resolution organ dosimetry for human exposure to low-frequency magnetic fields," *IEEE Trans. Magn.*, vol. 34, no. 3, pp. 708–718, May 1998.

[21] T. Dawson and M. Stuchly, "Analytic validation of a three-dimensional scalar-potential finite-difference code for low-frequency magnetic induction," *Appl. Comput. Electromagn. Soc. J.*, vol. 11, pp. 72–81, 1996.

[22] T. Noro and K. Wada, "A Univariate Outlier Detection Manual for Tabulating Statistical Survey," *Res. Mem. Stat.*, vol. 72, pp. 41–53, 2015.

[23] A. Hirata, Y. Takano, Y. Kamimura, and O. Fujiwara, "Effect of the averaging volume and algorithm on the *in situ* electric field for uniform electric- and magnetic-field exposures," *Phys. Med. Biol.*, vol. 55, no. 9, pp. N243–N252, May 2010.

[24] H. Tarao, H. Miyamoto, L. Korpinen, N. Hayashi, and K. Isaka, "Simple estimation of induced electric fields in nervous system tissues for human exposure to non-uniform electric fields at power frequency," *Phys. Med. Biol.*, vol. 61, no. 12, pp. 4438–4451, Jun. 2016.

[25] F. Freschi, L. Giaccone, and M. Mitolo, "Arc Welding Processes: An Electrical Safety Analysis," *IEEE Trans. Ind. Appl.*, vol. 53, no. 2, pp. 819–825, Mar. 2017.

Jose Gomez-Tames was born in Cartago, Costa Rica. He received the B.S. degree in electronics engineering from the Institute of Technology of Costa Rica, Cartago, Costa Rica, in 2007 and the M.S and Ph.D. degrees in medical system engineering from Chiba University, Chiba, Japan, in 2012 and 2015.

From 2007 to 2009, he was an Instructor with the Institute of Technology of Costa Rica. From 2015 to 2016, he was a Research Fellow of the Japan Society for the Promotion of Science, and also Visiting Researcher at the Singapore University of Technology and Design, Singapore. Since 2016, he has been a Research Assistant Professor in the Department of Computer Science and Engineering, Nagoya Institute of Technology, Nagoya, Japan. He is the author of more than 35 papers published in international journals and conference proceedings. His research interests include electromagnetics and neurostimulation for medical applications and assessment of human safety.

Dr. Gomez-Tames was a recipient of the Monbukagakusho Research Scholarship, JSPS Postdoctoral Fellowship, and the URSI Young Scientist Award. He is a member of the Institute of Electronics, Information and Communication Engineers of Japan, Bioelectromagnetics Society, and EMF Dosimetry Modeling Subcommittee of IEEE ICES.

Ilkka Lakkso (M'14) received the M.Sc.(Tech.) degree from Helsinki University of Technology, Espoo, Finland, in 2007, and the D.Sc.(Tech.) degree in electromagnetics from Aalto University, Espoo, in 2011.

Between 2013 and 2015, he has been a Research Assistant Professor and Research Associate Professor with the Department of Computer Science and Engineering, Nagoya Institute of Technology. Since 2015, he has been an Assistant Professor in electromagnetics in health technologies with Aalto University. He has authored more than 75 papers published in international journals and conference proceedings. His research interests include computational bioelectromagnetic modeling for assessment of human safety and biomedical applications.

Dr. Laakso has received several awards, including the Student Award in International Symposium on EMC, Kyoto, 2009; the Ericsson Young Scientist Award, 2011; and the Young Scientist Award in URSI Commission B International Symposium on Electromagnetic Theory, Hiroshima, Japan, 2013. He is the Secretary of Subcommittee "EMF Dosimetry Modeling" of the IEEE International Committee on Electromagnetic Safety and a member of the scientific expert group of International Commission on Non-Ionizing Radiation.

Yuto Haba received the B.S. and M.S. degrees in electrical and electronic engineering, in 2015 and 2017, from Nagoya Institute of Technology, Nagoya, Japan. His research focuses on dosimetry modeling.

Akimasa Hirata (S'98–M'01–SM'10–F'17) received the B.E., M.E., and Ph.D. degrees in communications engineering from Osaka University, Suita, Japan, in 1996, 1998, and 2000, respectively. He was a Research Fellow of the Japan Society for the Promotion of Science (JSPS Research Fellow) from 1999 to 2001, and also a Visiting Research Scientist at the University of Victoria, Canada in 2000. In 2001, he joined the Department of Communications Engineering, Osaka University as an Assistant Professor. In 2004, he joined the Department of Computer Science and Engineering, Nagoya Institute of Technology as an Associate Professor and now a Full Professor. His research interests are in electromagnetics and thermodynamics in biological tissue, waveguide analysis, EMC and EMI, and computational techniques in electromagnetics.

He is an editorial board member of Physics in Medicine and Biology, a member of the main commission and a chair of project group of International Commission on Non-Ionizing Radiation Protection (ICNIRP), and a member of Administrative Committee and a subcommittee (EMF Dosimetry Modeling) chair of IEEE International Committee on Electromagnetic Safety, and an expert of World Health Organization. He was also an Associate Editor of IEEE Transactions on Biomedical Engineering (from 2006 to 2012).

Dr. Hirata won several awards including Prizes for Science and Technology (Research Category 2011, Public Understanding Promotion Category 2014) by the Commendation for Science and Technology by the Minister of Education, Culture, Sports, Science and Technology, Japan, and IEEE EMC-S Technical Achievement Award. He is a Fellow of Institute of Physics, and a member of IEICE, IEE Japan, and Bioelectromagnetics Society (BEMS).

Dragan Poljak (SM'13) received the B.Sc., M.Sc., and Ph.D. degrees in electrical engineering from the University of Split, Split, Croatia, in 1990, 1994, and 1996, respectively. He is the Full Professor at Department of Electronics, FESB at the University of Split, and he is also Adjunct Professor at Wessex Institute of Technology (WIT), UK and member of WIT Board Directors. His research interests include frequency and time domain computational methods in electromagnetics, particularly in the numerical modelling of thin wire configurations, human exposure to electromagnetic radiation, biomedical applications of electromagnetic fields and magnetohydrodynamics. From 2011 to 2015 professor Poljak was the Vice-dean for research at the Faculty of electrical engineering, mechanical engineering and naval architecture. In 2011 professor Poljak became a member of WIT Bord of Directors. In June 2013 professor Poljak became a member of the Board of the Croatian Science Foundation.

Kenichi Yamazaki (M'95, SM'06) was born in Yokohama, Japan, on February 26, 1968. He received the B.S. degree in applied physics from the Tokyo University of Science, Tokyo, Japan, in 1990, and the M.S. and Ph.D. degrees in biomedical engineering from Hokkaido University, Sapporo, Japan, in 1992 and 2001, respectively. In 1992, he joined the Central Research Institute of Electric Power Industry (CRIEPI), Komae, Tokyo, Japan. He is currently a Deputy Associate Vice President and Leader of Lightning & Electromagnetic Environment Electric Research Section at CRIEPI, Yokosuka, Japan. In 2002 and 2003, he was a visiting scientist at the School of Electrical Engineering and Computer Science, Washington State University, Pullman, WA. His research interests include characterization of human exposure to low frequency electromagnetic fields, development of EMF exposure facilities for biological experiments, and power line electromagnetic compatibility. Dr. Yamazaki is a member of Bioelectromagnetics Society.